J Electr Eng Technol.2017; 12(4): 1357-1368
http://doi.org/10.5370/JEET.2017.12.4.1357

ISSN(Print) 1975-0102
ISSN(Online) 2093-7423

Robust Active Power Control of a Battery-Supported DSTATCOM to Enhance Wind Generation Power Flow

Mohammad Mahdianpoor*, Arash Kiyoumarsi†, Mohammad Ataei* and Rahmat-Allah Hooshmand*

Abstract – The lack of controllability over the wind causes fluctuations in the output power of the wind generators (WGs) located at the wind farms. Distribution Static Compensator (DSTATCOM) equipped with Battery Energy Storage System (BESS) can significantly smooth these fluctuations by injecting or absorbing appropriate amount of active power, thus, controlling the power flow of WGs. But because of the component aging and thermal drift, its harmonic filter parameters vary, resulting in performance degradation. In this paper, Quantitative Feedback Theory (QFT) is used as a robust control scheme in order to deactivate the effects of filter parameters variations on the wind power generation power smoothing performance. The proposed robust control strategy of the DSTATCOM is successfully applied to a microgrid, including WGs. The simulation results obviously show that the proposed control technique can effectively smooth the fluctuations in the wind turbines' (WT) output power caused by wind speed variations; taking into account the filter parameters variations (structural parameter uncertainties).

Keywords: Distribution static compensator, Quantitative feedback theory, Smoothing wind power fluctuation, Wind farm, Wind speed, Wind turbine

1. Introduction

Distributed Generation (DG) and Distributed Energy Storage (DES), generally known as Distributed Energy Resources (DERs), are small energy sources that can improve system reliability, if appropriately controlled. The intermittent nature of some renewable energy sources like photovoltaic [1, 2] and wind energy [3-5] adversely influences their related DG dynamics. The wind power, as an energy source with the fastest growing rate all around the world, is considered in this paper. It expands at a rate of 25-35 percent annually over the last decade [6]. The wind speed fluctuations can cause variations of the DG output power leading to problems such as system instability. These problems can be more severe in power systems with high wind energy penetration or in an island power network [7, 8]. It is worth noting that the problem of output power variation is more probable to arise when using fixed-speed wind turbines (FSWTs). This type of DG – having the advantages of cost effectiveness and robustness – uses the induction generators directly connected to the grid [7]. In order to overcome the problem, a DSTATCOM [9] equipped with an energy storage system (ESS) can be incorporated as an effective DES device which is able to exchange active power with the electric grid [10-3]. As discussed in [14], according to IEEE survey, BESS has the most growth over the other types of energy storage devices like flywheel or electrochemical capacitors. In [15] some projects of DSTATCOM with energy storage, which are implemented in the USA and Japan, have been considered.

There are some studies reported in the literature regarding the incorporation of different types of ESSs into the wind energy power generation. Batteries [16-20], Superconducting Magnetic Energy Storage (SMES) [21], Super-Capacitors (SC) [22] and Flywheel Energy Storage Systems (FESS) [23] are the main instances of these types. In [16], BESS is integrated into a wind power system that serves as an auxiliary source for it during the wind power fluctuations and/or load changes. The PI controller is used to manage the flow of power among the WT generator, ESS and the grid. However this structure can be used only for the voltage source converter (VSC)-based WGs. In [17, 18] connecting the BESSs in parallel with the WGs through converters, is proposed. In [17] this system is controlled by the artificial neural network controller to control the power injected into the grid during the wind speed variations. But the effect of converter harmonic filter on the equipment performance is not discussed. This is also the deficiency of the methods proposed in [19, 20]. In [19], the authors focus on designing the BESS for a wind-iesel off-grid power system to maximise the economic benefits and reliability of the power system. In [20] a wind-diesel power system is proposed- which applies a diesel generator together with a WT generator-

† Corresponding Author: Dept. of Electrical Engineering, Faculty of Engineering, University of Isfahan, Isfahan, Iran (kiyoumarsi@eng.ui.ac.ir)
* Dept. of Electrical Engineering, Faculty of Engineering, University of Isfahan, Isfahan, Iran (Mahdianpoor112@gmail.com, {Ataei, Hooshmand_r}@eng.ui.ac.ir)
Received: September 6, 2016; Accepted: March 20, 2017

to provide power for some loads. The BESS, controlled by PID controllers, is used there with the aim of regulating the isolated system frequency. The utilization of SMES is proposed in [21] in order to control the power flow in microgrids including WGs. The demerit is that the structure of the compensator is complicated. Moreover, the controller lacks robustness against uncertainties and variations of the components parameters. In [22] a wind farm equipped with the doubly fed induction generators (DFIG) and SCs is investigated. The control system operates such that the deviation between the available and desired active power output is compensated by the SC. The PI controllers are used for controlling the power flow of wind generation. In [23], a DSTATCOM/FESS with PI controller is utilized with a multi-level controller for integrating WGs into the power system.

The robustness of the control algorithm against uncertainties of the system plays an important role in the controller design process. In [24], a robust fuzzy-SA-IWD-PID controller for the DSTATCOM is introduced that uses a combination of fuzzy, simulated annealing (SA) and intelligent water drops (IWD) algorithms – instead of the trial-and-error method – for optimizing the PID controller parameters. Hence, the settling and rising times, the maximum overshoot and the steady-state error of the DSTATCOM's voltage step response can be decreased; but its design procedure is complicated and not easy to implement. The zero-set concept has been used in [25] to obtain the complete set of the STATCOM state feedback gains which cannot be performed by means of the optimization-based techniques. Thus, the robust design of a state feedback controller for a STATCOM is improved. In [26] a robust control scheme is proposed for the STATCOM through the Riccati equations, in order to improve the low voltage ride through (LVRT) capability of the FSWTs. But the design procedure is complicated and time consuming. In [27] fuzzy sliding-mode control algorithm is applied to control the STATCOM equipment under various faulted operating conditions. But, the robustness against equipment parameter variations is not clearly assessed.

In the above-mentioned works, the DSTATCOM controllers are designed for the fixed-values of filter parameters. It is obvious that component aging, thermal drift and saturation effects inevitably can cause variations in the system parameters; therefore, it is necessary to design a controller with an acceptable robustness with respect to the system parameters variations.

The QFT is widely applied in many control applications [28] as a robust method which is relatively easy in design. In [29], some advantages of the QFT scheme are briefed as: a robust design can be achieved with no sensitivity to structured plant parameters variations; one robust design can exist for the full operating envelope; design limitations are obvious during the design process; the achievable performance specifications can be found in the early design stage; if changes in the specifications are needed, a redesign can be made easily through QFT CAD package; the structure of the controller is determined straightforward; the development of the envelope design requires a shorter time; and, optimizing the controller parameters is simpler than that of the PI controllers. For providing a robust controller for DSTATCOM and as the novelty of this article, QFT method is applied on a BESS supported DSTATCOM for smoothing the output power of FSWGs such that the DSTATCOM harmonic filter parameters variations in a range of ±30% do not affect its power smoothing performance. Attempt is made in this study to apply a continuous-time uncertain transfer function model which has parametric uncertainties of the harmonic filter parameters.

The remainder of the paper is organized as follows: the general structure of the DSTATCOM is provided in Section 2. In Section 3, the inverter harmonic filter design is briefly described. The basis of the proposed control method is described in Section 4. Section 5 includes the DSTATCOM active power control algorithm. Finally, the simulation results are provided in Section 6, which show the capability of the DSTATCOM with QFT controller in improving the quality of power generation in microgrids. The parameters of the compensator harmonic filter, WT and wind model which are used in the simulations are listed in the appendices A, B and C respectively. Appendix D contains almost all abbreviations and acronyms that are used in this article.

2. The DSTATCOM Components

As observed in Fig. 1, the DSTATCOM consists of an injection transformer, a VSC, an inverter output filter, and an ESS connected in parallel with a DC-link capacitor. A battery is used as the ESS. A VSC, consisting of 12 switches (three full H-bridge converters), is used in order to compensate for each phase, individually. In fact, the VSC performs as three single-phase converters so that it can cope with zero-sequence current under unbalanced conditions. The VSC generates some high-frequency harmonics due to switching functions. Thus, a filter is designed for high-power VSCs with the switching frequency of 10 kHz. In this paper, an LCL filter is used for this purpose.

3. Harmonic Filter Design (The LCL Filter)

The DSTATCOM injects harmonics to the grid; hence, the design of an appropriate filter to effectively attenuate such high-frequency switching harmonics, is essential [30]. Many of the existing DSTATCOMs' structures use a simple first-order L filter; however, the L filter is bulky and inefficient, and does not meet the specified requirements

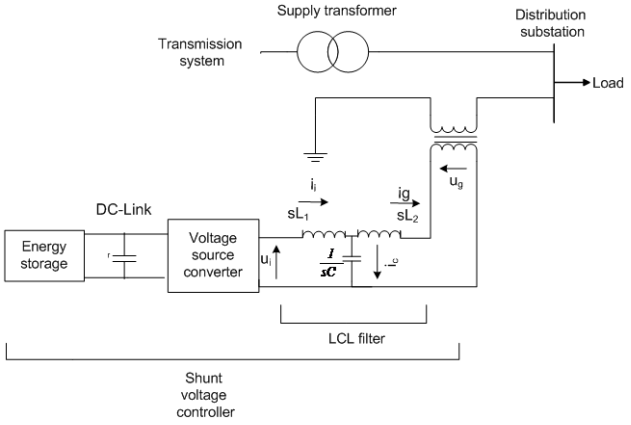

Fig. 1. The distribution system with the DSTATCOM device

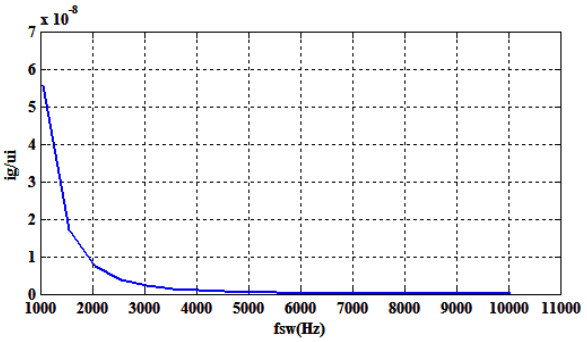

Fig. 2. Variation of (i_g/u_i) with respect to f_{sw} for the filter parameters of Table A.1

for the switching ranges of mid- to high-power inverter applications [30].

In this article, the designed filter is of the LCL filter pattern, in order to meet the grid interconnection standards at a significantly smaller size and cost [31, 32]. The per-phase equivalent circuit of an LCL filter is shown in Fig. 1.

According to Fig. 1 the inverter output voltage and current are represented by u_i and i_i, and the grid voltage and current are denoted by u_g and i_g, respectively. The switching frequency is f_{sw}. The grid is assumed to be stiff enough such that it can be considered as an almost ideal voltage source. The transfer function of the LCL filter is yielded as follows:

$$(i_g(s)/u_i(s)) = (1/s^3 L_1 L_2 C + s(L_1 + L_2)) \quad (1)$$

where, L_1, L_2 and C are the LCL filter inductances and capacitance, respectively. Equation (2) determines the minimum value of L which is equal to (L_1 + L_2) for which the IEEE 519-1992 standard requirements are met for current ripple at the switching frequency [31]. The size of L depends on the resonance frequency ω_r.

$$L = (1/(\omega_{sw} |(i_g(s)/u_i(s)) |1 - (\omega_{sw}^2/\omega_r^2)|)) \quad (2)$$

By applying L and ω_r, the value of C is determined as follows:

$$\omega_r^2 = 4/LC \quad (3)$$

where, ω_r is a constant, while, the values of L and C can be adjusted. The design decision in selecting the resonance frequency depends on the bandwidth of the closed-loop system. Since this bandwidth is decided by the filter elements and the control algorithm, an initial estimate of the maximum possible system bandwidth is required in advance. This bandwidth is assumed to be one-tenth of the switching frequency of the VSC [31]. If the value of computed L from (2) is very small and/or C is greater than 1 pu, (3) is applied to scale L up and C down. The closed-loop system will be unstable if some voltage/current harmonics coincide around the resonance frequency. To overcome this drawback, a damping resistance is located in parallel with the LCL filter capacitor [31]. The parameters of this designed LCL filter are tabulated in Table A.1 of Appendix A. The ratio of i_g to u_i is decreased whenever the switching frequency increases, Fig. 2. Since the filter is designed for high-power VSCs with the switching frequency of 10 kHz [31], in Fig. 2 it is observed that this ratio is equal to zero in this design.

4. The Closed-loop Control by Applying QFT Controller

The QFT applies a feedback such that the appropriate system performance can be achieved despite the plant uncertainties [33]. The QFT design procedure, involves three basic steps: The QFT bounds are computed, the compensator G and pre-filter F are designed [29] and the design is analysed. In the first step, the appropriate specifications of the open-loop function are converted into magnitude and phase constraints which are applied in nominal open-loop function. The QFT bounds are computed based on these constraints. After that, in the loop shaping stage, a nominal open-loop function is yielded that satisfies the constraints and achieves the nominal loop stability. In order to guarantee that the requirements of the design are met at the defined frequency range, the design analysis should be run. The block diagram of the control system and this proposed QFT flowchart is shown in parts (a) and (b) of Fig. 3, respectively, where in part (a), the R(s), F(s), G(s), P(s), Y(s) are the DSTATCOM reference signals, pre-filter, controller, plant model, and output signal Laplace transforms, respectively.

The first primary control objective in QFT design is the stability with reasonable margins of:

$$|PG(j\omega)/(1+PG(j\omega))| \le 1.2, \quad \omega > 0 \quad (4)$$

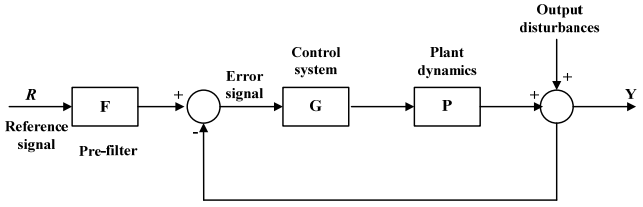

(a)

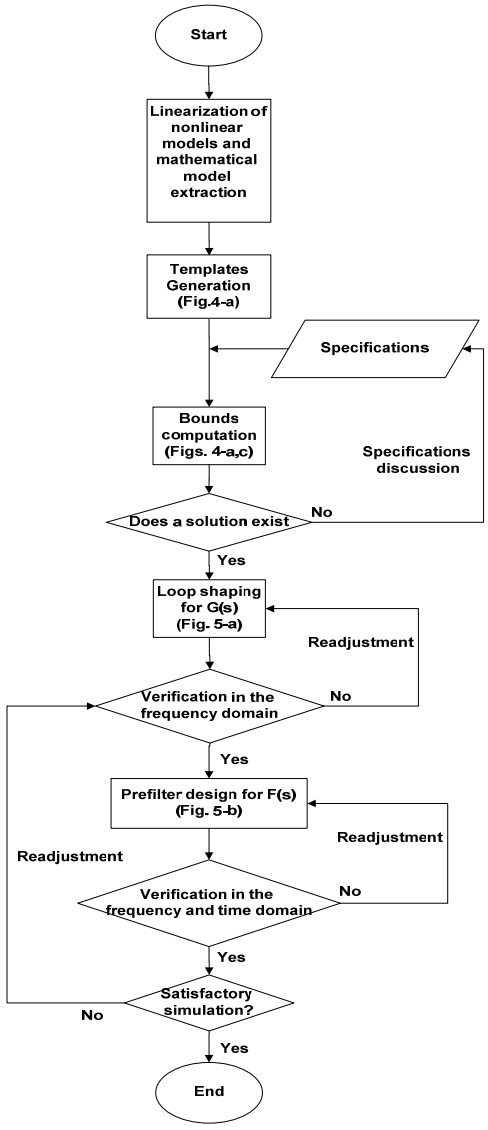

(b)

Fig. 3. (a) Control block diagram of the system in QFT design and (b) QFT flowchart

where, P and G are the DSTATCOM plant model and the QFT controller to be designed, respectively. The second control objective is the robust tracking provided that,

$$\left| a(j\omega) \right| \le \left| F(j\omega)PG(j\omega)/(1+PG(j\omega)) \right| \le \left| b(j\omega) \right| \quad \omega < 2000 \text{ rad/s} \tag{5}$$

where, $a(j\omega)$ and $b(j\omega)$ are the unit step response output margins. The stability margins are the closed-loop system specifications with constant gain, drawn in Nichols chart. Obviously, the system response overshoot should be restricted on a specific value, which is set to 1.2 here, as proposed by Horowitz [33].

The DSTATCOM plant model is the LCL filter transfer function given in (1), re-written in (6), which is the ratio of the DSTATCOM current injected to the grid and the DSTATCOM inverter output voltage (Fig. 2).

$$P = 1/(s^3 L_1 L_2 C + s(L_1 + L_2)) \tag{6}$$

A continuous-time uncertain transfer function model can have a structure mode of parametric, non-parametric or a combination of both. As mentioned earlier, attempt is made in this study to apply a continuous-time uncertain transfer function model which has parametric uncertainties. Its type of uncertainty implies the knowledge of transfer function parameters variations. In this particular design where the nominal values are L_1=20 mH, L_2=1mH, C=25μF, it is assumed that the filter parameters variations are within 14 to 26 mH for L_1 value range, 0.7 to 1.3 mH for L_2 value range and 17.5 to 32.5 μF for C value range; indicating a 30% parameter variation.

In order to design a QFT controller, the plant dynamics should be defined in terms of its frequency response, since the QFT works with frequency-domain arithmetic. Consequently, the term "template" is used, defined as a set of an uncertain plant's frequency responses at a given frequency. The performance bandwidth and the templates shape determine this frequency range. The margin bounds up to the frequency where the shape of the plant template becomes relatively invariant with respect to frequency are calculated. For DSTATCOM model in this study, with ω at approximately 2000 rad/s, the template shape becomes almost fixed. The plant templates at some frequencies are shown in Fig. 4(a).

To find the output margin (*i.e.*, b(s) in (5)) a conventional second-order system is considered with the overshoot and settling time values of 20% and 0.002 seconds, respectively, as an acceptable step response output high margin. In order to yield the transfer function of a(s), the main factor is the settling time. So a first-order transfer function with time constant (τ) equal to 0.005 seconds is determined as an acceptable low margin step response output, Fig. 4(b).

For the system to have appropriate characteristics in high frequencies the distance between the upper and lower limit bode diagrams [33] should be increased, Fig. 4(c). This increase in distance can be achieved by adding one zero- distanced from the imaginary axis- to b(s) and adding two poles- distanced from the imaginary axis- to a(s), simultaneously. Addition of the latter poles will increase the lower bode diagram slope in high frequencies. Through this procedure, the margins' transfer functions will be yielded, by trial and error, as follows:

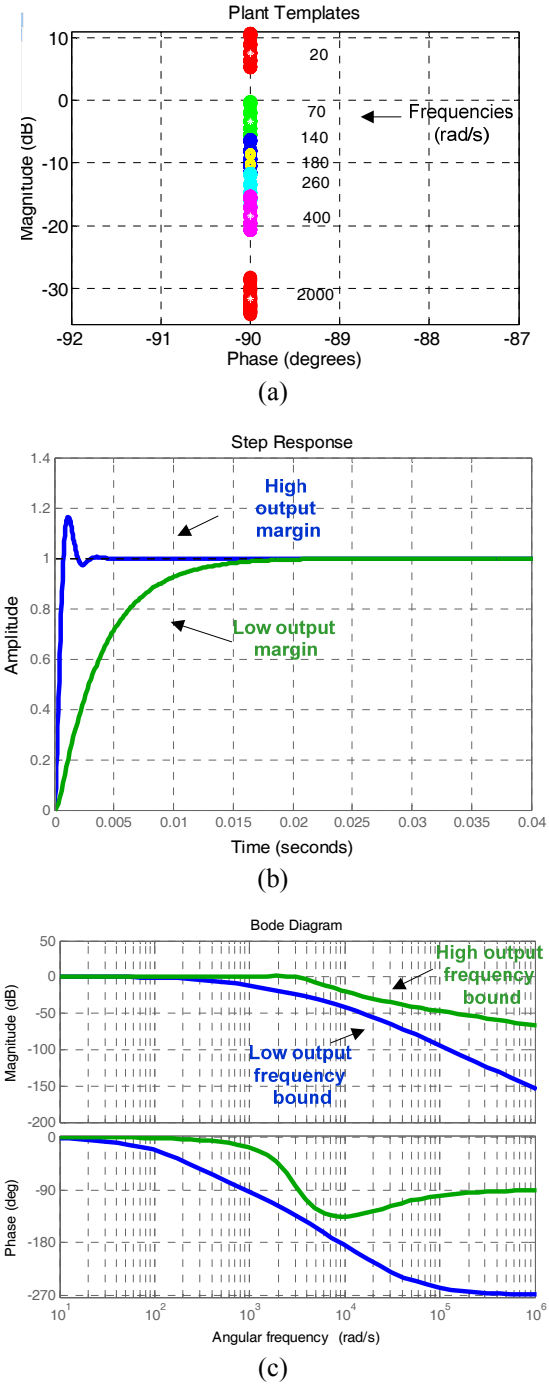

Fig. 4. (a) Templates in several frequencies (rad/sec) (b) step and (c) frequency responses of the two bounds

$$b(s) = (450s + 9*10^6)/(s^2 + 3000s + 9*10^6)$$
$$a(s) = 2*10^{10}/(s^3 + 24000*s^2 + 8.1*10^7 s + 2*10^{10}) \quad (7)$$

According to the desired performance specifications, the disturbance rejection bounds are computed through the QFT method, followed by obtaining the stability bounds (U-counters) leading to the design of a nominal loop function (named loop shaping) meeting its bounds. The nominal loop transfer function is the product of the

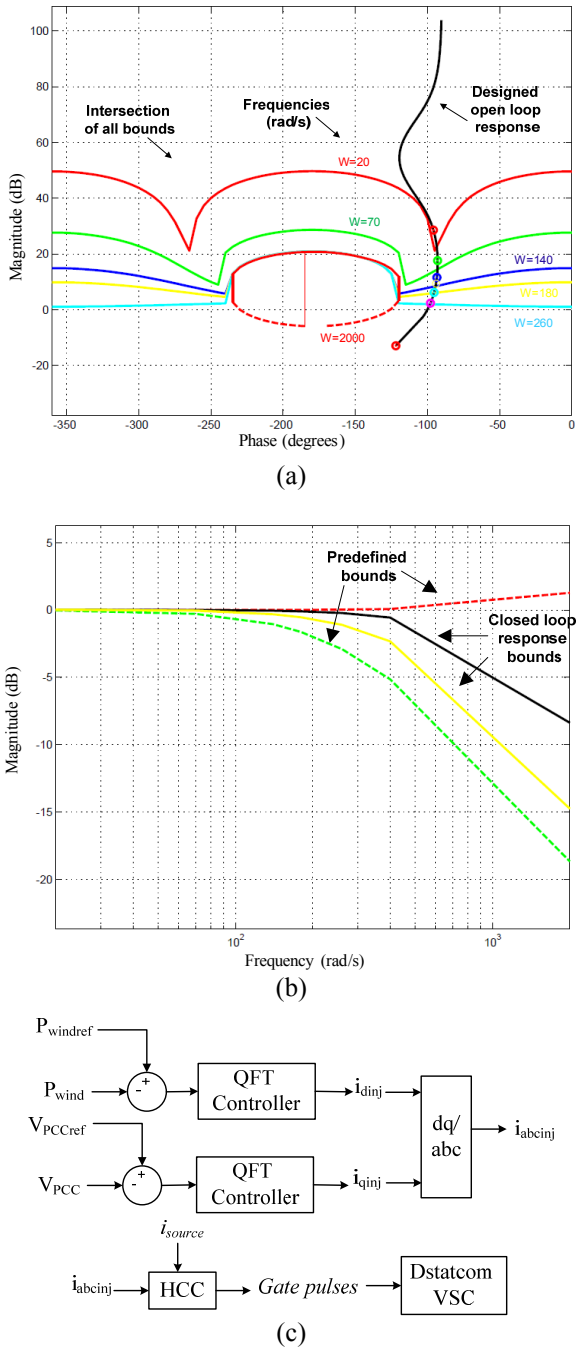

Fig. 5. (a) The QFT loop-shaping (frequencies in rad/sec) (b) Prefilter design and (c) the overall controller block diagram

nominal plant (P) and the controller transfer functions (G - that should be designed). For the nominal open-loop to satisfy all bounds, the loop transmission related to each frequency should be placed either on or over the respective frequency bounds. This task is carried out by choosing the controller zeros and poles properly, through the QFT toolbox of MATLAB software [34].

Before the loop shaping process, all bounds should be shown in one Nichols chart and their intersection should

be chosen for the loop shaping process. The loop shaping procedure, which results in the controller transfer function of (8), is shown in Fig. 5(a).

When designing a controller for robust tracking performance, in order to ensure that the closed-loop response is between the predefined bounds shown in Fig. 4(c), a pre-filter should be designed. Setting value 1– by trial and error– for pre-filter assures this condition, Fig. 5(b), which is obtained through QFT toolbox of MATLAB software [29];

$$G(s) = (2.363s^2 + 26265s + 76919) / (s^2 + 2354.9s + 2353.9) \quad (8)$$

It is important to notice that the speed at which a QFT design can be performed is heavily influenced by the experience of the user. Nevertheless, the MATLAB toolbox for QFT reduces the required skill and experience for loop shaping in QFT.

5. The Proposed DSTATCOM Active Power Control Algorithm

The block diagram of this proposed control strategy for the DSTATCOM is shown in Fig. 5(c). In this block diagram, $P_{windref}$ is the reference WG active power signal that should be injected through WT system into the network. The P_{wind} is the measured WG active power. The V_{WT} is the measured WG terminal phase voltage and V_{WTref} is its reference value. The error signals of active power and terminal voltage are sent to the QFT controllers formulated in (8) and signals i_{dinj} and i_{qinj} are yielded to compensate for the power and the voltage disturbances, respectively. The dq/abc transformation block is applied to yield the three-phase current signals that should be injected by the DSTATCOM. To determine the command signals for the DSTATCOM inverter, the reference signal $i_{DSTATCOMref}$ and the measured DSTATCOM current $i_{DSTATCOM}$ are applied to Hysteresis Current Control (HCC)-block [35], where they are compared with each other. Finally, the gate signals are produced by the HCC block and sent to the DSTATCOM VSC, Fig. 1.

6. Simulation Results

6.1 Test system

The IEEE standard 13-bus industrial system, Fig. 6(a), is applied as the test system. The test system is implemented in PSCAD/EMTDC software. The control method of Fig. 5(c) is used to control the DSTATCOM. The DSTATCOM is a 12-pulse inverter whose phases can be controlled separately. Thus, the DSTATCOM acts as three single phase converters so that it can inject zero-sequence current.

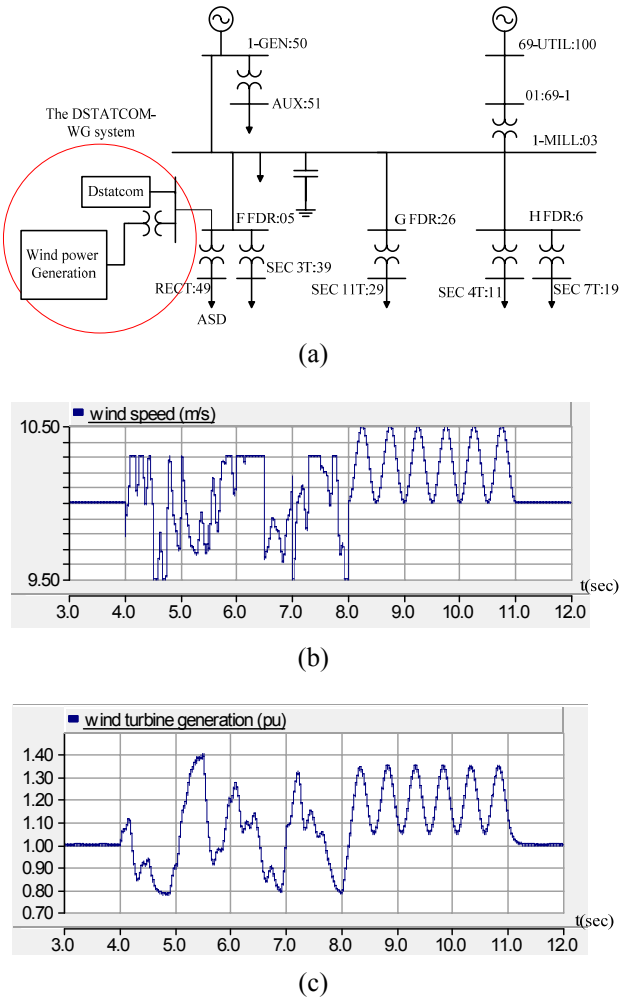

Fig. 6. (a) Test system under study [36](b) Wind speed fluctuations and (c) the resulting electric power fluctuations without compensator

The plant is fed from a utility supply at 69 kV and the local plant distribution system operates at 13.8 kV. The local (in-plant) generator is represented as a simple Thévenin equivalent circuit with the internal voltage of 13.8∠-1.52° kV, determined from the converged power flow solution. The equivalent impedance is the sub-transient impedance and equals to 0.0366+j1.3651 Ω. The plant power factor correction capacitors are rated at 6000 kVAr. As is typically assumed, the leakage and series resistance of the bank are neglected in this study. The detailed description of the system is given in [36]. A WG coupled with a DSTATCOM is implemented in the system. The DSTATCOM controls the active power flow from WT bus to bus "05:FDR F" of the grid and includes a 0.5 MW/1 MWh lithium-ion BESS [37]. It is noticeable that the peak of power oscillations is 0.4 MW in the simulations. The WG uses a squirrel-cage-type induction generator. The WG is modelled with blocks of an induction generator and a WT available in the PSCAD library with the parameters given in Table B.1, Appendix B.

6.2 A suitable profile for variation of wind speed

As shown in Fig. 6(b), two wind models are considered in this study, which are available in PSCAD/EMTDC software: the "Noise" component and the "Gust" component. The WG operates at a mean wind speed of 10m/s that from t=4 to t=8 sec, the noise component is also applied. The equations used for the random noise generation in PSCAD software are as follows:

$$V_{wn} = 2\sum_{i=1}^{N}(\sqrt{S_v(w_i)DW}\cos(w_i t + \phi_i)) \tag{9}$$

in which,

$$S_v(w_i) = \frac{2.K.N_0.F_0^2.|w_i|}{\pi^2\left[1+\left(\frac{F_0 w_i}{u.\pi}\right)^2\right]^{3/4}}, \quad w_i = (i-0.5)DW$$

In the above equations DW is the noise amplitude controlling parameter, which is a random variable on the interval 0 to 2, φ is a random variable with uniform probability density on the interval 0 to 2π. K is the surface drag coefficient, N_0 is the probability density function counter limit (an integer between 0 and 50), F_0 is the turbulence scale, and u is the mean wind speed value. The parameters according to noise wind component are moreover given in Table C.1, Appendix C. After the noise component, from t=8 to t=11 sec the "Gust" component is applied which is a sinusoidal component with peak-to-peak value of 0.5.

6.3 Output power smoothing in the face of parametric uncertainty

The wind power generation without DSTATCOM compensation is shown in Figs. 6(c), 7(a) and 9(a). As can be seen in the figure, the wind speed variations cause significant fluctuations in the active power injected by the WG. The base MVA for per-unit system is 1 MVA in these figures.

The injected power of WG-DSTATCOM coupled system using PI controller is shown in Fig. 7(b)-(d). The PI parameters for voltage control loop are k_p=15 and k_I=0.1. Also for active power control loop, they are k_p=k_I=0.1. These optimal parameters are derived by the support of MATLAB PID tuner with Ziegler-Nichols algorithm. In Fig. 7(a), fluctuations in the active power injected by the WG are shown again for comparison with DSTATCOM-compensation case. As shown in this figure, the wind speed variation causes the output power to increase up to 40% nominal value which will make the system instable if not controlled. In Fig. 7(b) nominal filter parameters designed in Section 3 and tabulated in Table A.1, Appendix A, are used in DSTATCOM harmonic filter. In Fig. 7(c), filter parameters are increased by 30%, and, in Fig. 7(d), filter parameters are decreased by 30%. It is clearly understood from these parts of Fig. 7 that application of DSTATCOM is useful to limit the power oscillation amplitudes effectively and help for the system stability (oscillation amplitude has decreased from the maximum value of 40% to 15%), but the performance of the

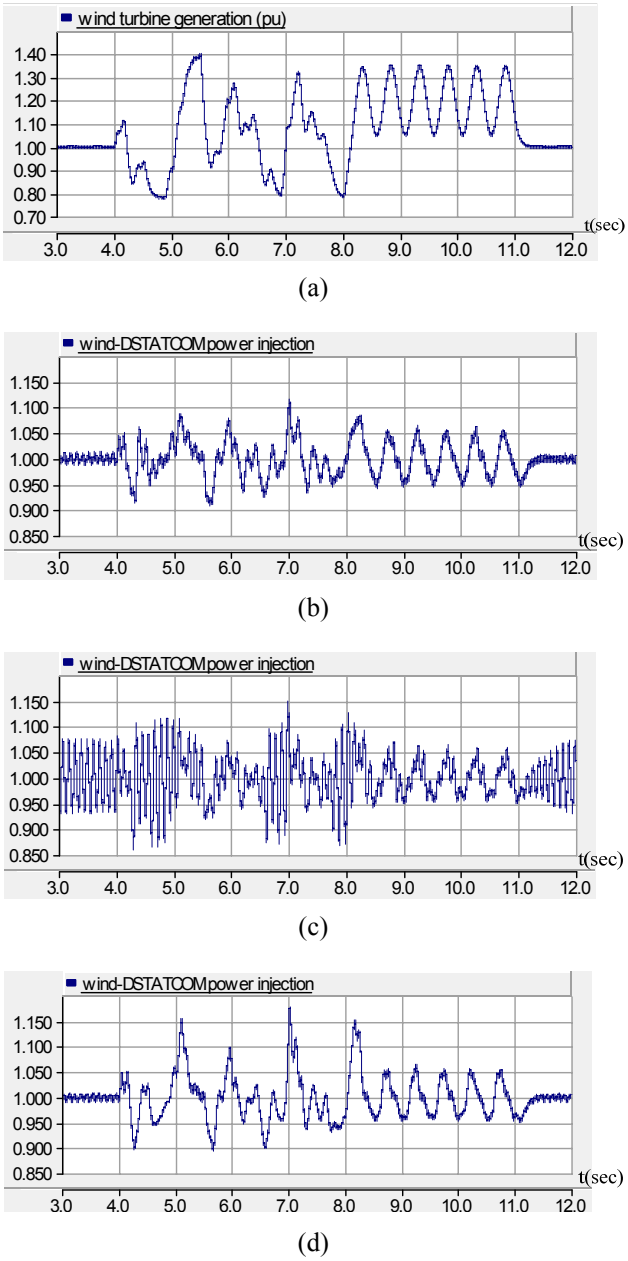

Fig. 7. The injected power of (a) WG without DSTATCOM (b) WG-DSTATCOM with PI controller and nominal filter parameters tabulated in Table A.1, appendix A, (c) WG-DSTATCOM with PI controller and filter parameters have been increased by 30%, (d) WG-DSTATCOM with PI controller and filter parameters have been decreased by 30%

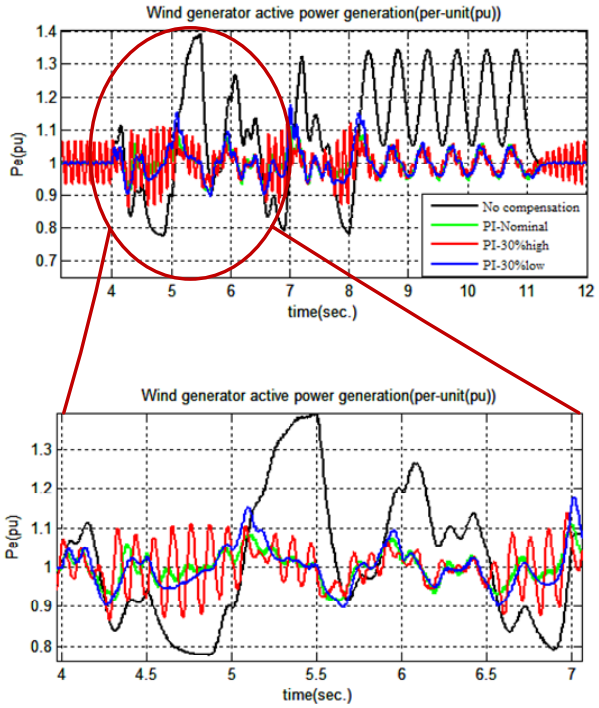

Fig. 8. WG active power variations caused by wind speed variations in four cases: no compensation and PI controlled WG-DSTATCOM with nominal, 30% high and 30% low filter parameters

compensator is affected by the filter parameters variations. Particularly, in part "b" both the frequency of output oscillations and their amplitudes are augmented. On the other hand, in part "c" amplitude augmentation of the oscillations is more severe than part "b". As can be seen, in some parts of the waveform, the amplitude of oscillations reaches to 1.15 pu (*i.e.*, about 15% increase in the output power of wind generator). These figures are obtained in PSCAD/EMTDC environment. In Fig. 8 all cases of Fig. 7 are shown in one figure by the help of MATLAB software, for better comparison. The enlarged part in Fig. 8 clearly shows the effects of filter parameters variations in the WG-DSTATCOM output power.

The QFT controller designed in Section 4 as in (8) is used with the same system and the resulting output power is shown in Fig. 9. In Fig. 9(a), fluctuations in the active power injected by the WG is shown for comparison with DSTATCOM-compensation case. In Fig 9(b) nominal filter parameters designed in Section 3 and mentioned in Table A.1 in Appendix A are used. In Fig. 9(c), filter parameters are increased by 30% and in Fig. 9(d), filter parameters are decreased by 30%. It can be clearly observed that not only the QFT controller has dampened the oscillation amplitudes to a value less than 3%, but it also has almost no change in performance with respect to filter parameters variations. Note that the scaling of the power axis has changed from (0.85)-(1.15) pu to (0.98)-(1.03) pu for the QFT controller outputs (*i.e.*, Fig. 9).

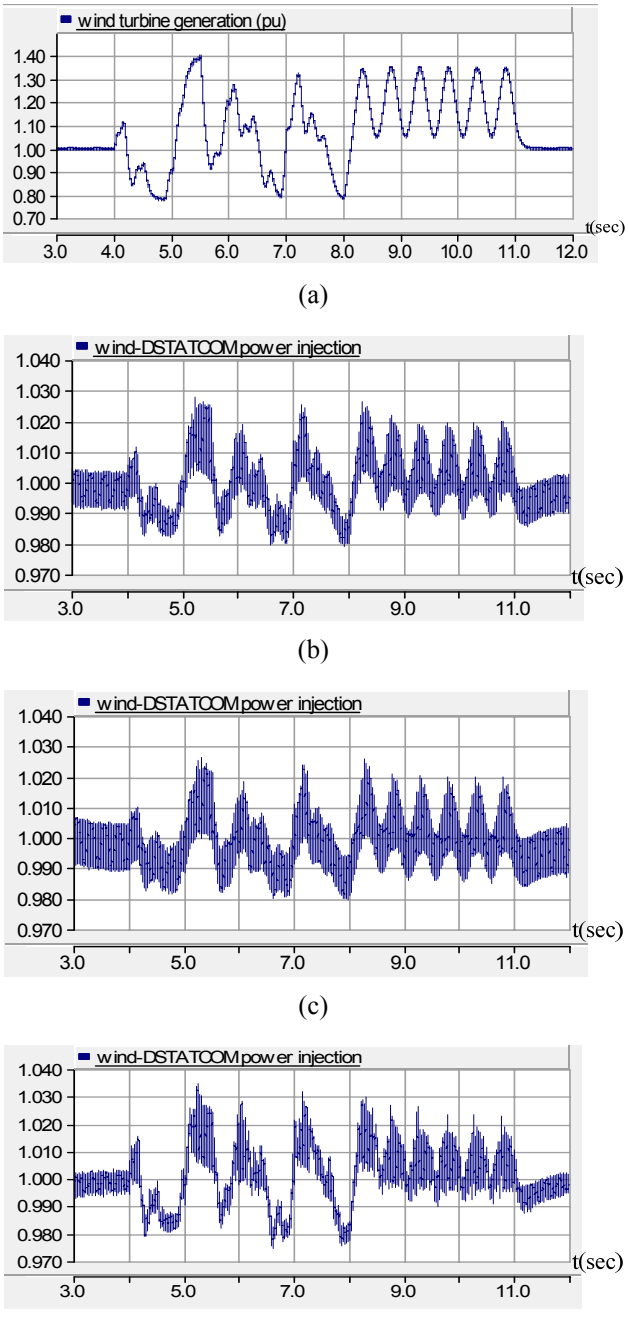

Fig. 9. The injected power of (a) WG without DSTATCOM, (b) WG-DSTATCOM with QFT controller and nominal filter parameters tabulated in Table A.1, appendix A, (c) WG-DSTATCOM with QFT controller and filter parameters have been increased by 30%, (d) WG-DSTATCOM with QFT controller and filter parameters have been decreased by 30%

These figures are obtained in PSCAD/EMTDC environment. In Fig. 10 all cases of Fig. 9 are shown in one figure by the help of MATLAB software, for better comparison. The enlarged part in Fig. 10 clearly shows that filter

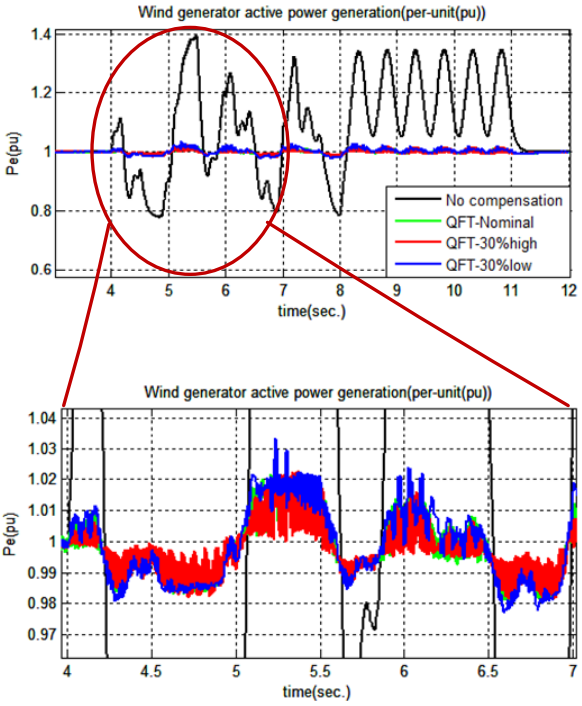

Fig. 10. WG active power variations caused by wind speed variations in four cases: no compensation and QFT controlled WG-DSTATCOM with nominal, 30% high and 30% low filter parameters

Table 1. Comparison between the simulation results of PI and QFT methods

Parameters of harmonic filter	PI controller	QFT controller
filter parameters increased by 30%	Both the frequency of output oscillations and their amplitudes are augmented compared to nominal values of filter parameters. Amplitude of oscillations is dampened to the value of 7%.	Oscillation amplitudes are decreased to 3% and there is no significant change comparing to the case of nominal filter parameters.
filter parameters decreased by 30%	Amplitude augmentation of the oscillations is more severe than the case of increased filter parameters but the frequency of oscillations is less. About 15% increase has happened in the output power of WG in some parts of the waveform.	Oscillation amplitudes are decreased to 3% and there is no significant change comparing to the case of nominal filter parameters.

parameters variations has almost no actual effect on the QFT controlled WG-DSTATCOM output power.

As can be observed in the simulation results, by incurporating the DSTATCOM/BESS, power fluctuations of WG are reduced but if QFT is used as the controller, not only the compensator response has a satisfactory waveshape but it is also almost independent of the filter parameter variations in the range of ±30%. A comparison between the simulation results of PI and QFT controller is shown in Table 1.

7. Conclusion

In this paper, QFT method is used as a robust controller to control a battery-supported DSTATCOM in order to smooth the WG output power fluctuations caused by unpredictable fluctuations in the wind speed. It is shown that filter parameter variations, due to aging or temperature, can change the response of a DSTATCOM when incurporating a non-robust controller. The QFT controller's structure is determined straightforward and its design is not complicated or time consuming. Also optimizing the controller parameters is not a problem like in the PI controllers. The simulation results show that whenever the filter parameters are varied by 30%, compared to their nominal values, in the case of a non-robust controller; the frequency of output oscillations and their amplitudes change. However, after incorporating the designed QFT controller, the oscillation amplitudes are decreased to 3% and there is almost no significant change in the output with filter parameter variations in the range of 30%.

Acknowledgements

Special thanks are dedicated to Dr. Eskandar Gholipour for his comments and modifications that indeed improved the contents of the manuscript. The authors would also like to appreciate supports of Mr. Mostafa Malekpour for his suggestions during the preparation of this paper. Valuable comments from two anonymous reviewers indeed helped to significantly improve and enhance the contents of this research. We would really appreciate their comprehensive attentions and vital considerations.

References

[1] M. Datta, T. Senjyu, A. Yona, T. Funabashi and C. H. Kim, "Design of Intelligent Control for Stabilization of Microgrid System," *Int. J. Elec. Power,* vol. 82, pp. 569-578, 2016, doi:10.1016/j.ijepes.2016.04.030.

[2] S. Surender Reddy and P. R. Bijve, "Day-Ahead and Real Time Optimal Power Flow considering Renewable Energy Resources," *Int. J. Elec. Power*, vol. 82, pp. 400-408, 2016, doi: 10.1016/j.ijepes.2016.03.033

[3] J. Wang, F. Zhang and F. Liu, "Hybrid Forecasting Model-based Data Mining and Genetic Algorithm-Adaptive Particle Swarm Optimisation: a Case Study of Wind Speed Time Series," *IET Renew. Power Gen.*, vol. 10, no. 3, pp. 287-298, 2016, doi:10.1049/iet-rpg.2015.0010.

[4] W. Na, W. Quan and S. Sheng, "Long Term Variation Trend of Wind and its Impact Upon Wind Power Generation in Taiwan," *Journal of Electrical Engineering and Technology*, vol. 9, no. 3, pp. 782-788, May 2014, doi: 10.5370/JEET.2014.9.3.782.

[5] L. B. Shi, L. Kang, L. Z. Yao and S. Y. Qin, "Effects of Wind Generation Uncertainty and Volatility on Power System Small Signal Stability," *Journal of Electrical Engineering and Technology*, vol. 9, no. 1, pp. 60-70, Jan. 2014, doi: 10.5370/JEET.2014.9.1.060.

[6] T. Zhou and B. François, "Energy Management and Power Control of a Hybrid Active Wind Generator for Distributed Power Generation and Grid Integration," *IEEE Trans. Ind. Elec*., vol. 58, no. 1, pp. 95-104, 2011.

[7] T. Ackermann, "Wind Power in Power Systems" (John Wiley & Sons, London, UK, 2005).

[8] L. Shi, Sh. Sun, L. Yao, Y. Ni and M. Bazargan, "Effects of Wind Generation Intermittency and Volatility on Power System Transient Stability," *IET Renew. Power Gen*., vol. 8, no. 5, pp. 509-521, 2014, doi: 10.1049/iet-rpg.2013.0028.

[9] R. Sarrias, C. González, L. M. Fernández, C. A. García and F. Jurado, "Comparative Study of the Behavior of a Wind Farm Integrating Three Different FACTS Devices," *Journal of Electrical Engineering and Technology*, vol. 9, no. 1, pp. 1258-1268, Jan. 2014, doi: 10.5370/JEET.2014.9.4.1258.

[10] B. Ronner, P. Maibach and T. Thurnherr, "Operational Experiences of STATCOMs for Wind Parks," *IET Renew. Power Gen*., vol. 3, no. 3, pp. 349-357, 2009, doi: 10.1049/iet-rpg.2008.0075.

[11] K. Zhang, C. Mao, J. Xie, J. Lu, D. Wang, J. Zeng, X. Chen and J. Zhang, "Determination of Characteristic Parameters of Battery Energy Storage System for Wind Farm," *IET Renew. Power Gen*., vol. 8, no. 1, pp. 22-32, 2014, doi:10.1049/iet-rpg.2012.0385.

[12] G. O. Suvire and P. E. Mercado, "Active Power Control of a Flywheel Energy Storage System for Wind Energy Applications," *IET Renew. Power Gen*., vol. 6, no. 1, pp. 9-16, 2012, doi:10.1049/iet-rpg. 2010.0155.

[13] X. Li, "Fuzzy Adaptive Kalman Filter for Wind Power Output Smoothing with Battery Energy Storage System," *IET Renew. Power Gen*., vol. 6, no. 5, pp. 340-347, 2012, doi:10.1049/iet-rpg.2011.0177.

[14] P. Khayyer and Ü. Özgüner, "Decentralized Control of Large-Scale Storage-Based Renewable Energy Systems," *IEEE Trans. Smart Grid*, vol. 5, no. 3, pp. 1300-1307, 2014.

[15] A. Jones, "Grid Connection of Renewable Energy," Innovative Smart Grid Technologies Conference Europe (ISGT Europe), Gothenburg, Sweden, pp. 1-4, Oct. 2010, DOI: 10.1109/ISGTEUROPE.2010.5638908

[16] A. Abedini and H. Nikkhajoei "Dynamic Model and Control of a Wind Turbine Generator with Energy Storage," *IET Renew. Power Gen*., vol. 5, no. 1, pp. 67-78, 2011.

[17] S. Kurian, S. T. Krishnan and E. P. Cheriyan, "Real Time Implementation of Artificial Neural Networks-based Controller for Battery Storage Supported Wind Electric Generation," *IET Gener. Transm. Distrib*., vol. 9, no. 10, pp. 937-946, 2015, doi:10.1049/iet-gtd. 2014.0544.

[18] Z. Wei, B. Y. Moon and Y. H. Joo, " Smooth Wind Power Fluctuation Based on Battery Energy Storage System for Wind Farm," *Journal of Electrical Engineering and Technology*, vol. 9, no. 6, pp. 2134-2141, Nov. 2014, doi: 10.5370/JEET.2014.9.6.2134.

[19] L. Guo, Z. Yu, C. Wang, F. Li, J. Schiettekatte, J. C. Deslauriers and L. Bai, "Optimal Design of Battery Energy Storage System for a Wind-diesel Off-grid Power System in a Remote Canadian Community," *IET Gener. Transm. Distrib*., vol. 10, no. 3, pp. 608-616, 2016, doi: 10.1049/iet-gtd.2015.0190.

[20] R. Sebastián, "Application of a Battery Energy Storage for Frequency Regulation and Peak Shaving in a Wind Diesel Power System," *IET Gener. Transm. Distrib*., vol. 10, no. 3, pp. 764-770, 2016, doi: 10.1049/iet-gtd.2015.0435.

[21] M. G. Molina and P. E. Mercado, "Power Flow Stabilization and Control of Microgrid with Wind Generation by Superconducting Magnetic Energy Storage," *IEEE Trans. Power Electron*., vol. 26, no. 3, pp. 910-922, 2011,

[22] L. Qu and W. Qiao, "Constant Power Control of DFIG Wind Turbines with Super Capacitor Energy Storage," *IEEE Trans. Ind. Appl*., vol. 47, no. 1, pp. 359-367, 2011.

[23] G. O. Suvire and P. E. Mercado, "DSTATCOM with Flywheel Energy Storage System for Wind Energy Applications: Control Design and Simulation," *Elsevier-Electr. Power Syst. Res*., vol. 8, no. 3, pp. 345-353, 2010.

[24] H. Bagheri Tolabi, R. Hosseini and M. R. Shakarami, "A Robust Hybrid Fuzzy-simulated Annealing-intelligent Water Drops Approach for Tuning a Distribution Static Compensator Nonlinear Controller in a Distribution System," *T&F Eng. Optimiz*., pp. 1-20, 2015, doi: 10.1080/0305215X.2015.1080579.

[25] V. Spitsa, A. Alexandrovitz and E. Zeheb, "Design of a Robust State-feedback Controller for a Dstatcom using a Zero Set Concept," *IEEE Trans. Power Del*., vol. 25, no. 1, pp. 456-467, 2010.

[26] M. J. Hossain, H. R. Pota and R. A. Ramos, "Robust Statcom Control for the Stabilisation of Fixed Speed Wind Turbines during Low Voltages," *Renew. Energ*., vol. 36, no. 11, pp. 2897-2905, 2011.

[27] S. K. Routray, N. Nayak and P. K. Rout, "A Robust Fuzzy Sliding Mode Control Design for Current Source Inverter based STATCOM Application," *Elsevier, Procedia Technology*, vol. 4, no. 11, pp. 342-349, 2012.

[28] A. Khodabakhshian, M. Mahdianpoor and R. Hooshmand, "Robust Control Design for Multi-functional DVR Implementation in Distribution Systems using Quantitative Feedback Theory," *Elsevier*

- *Electr. Power Syst. Res*., vol. 97, pp. 116-125, 2013.
[29] C. H. Houpis, S. J. Rasmussen and M. Garcia-Sanz, "Quantitative Feedback Theory: Fundamentals and Applications," (CRC press, 2006, taylor and francis group)
[30] IEEE Standard 1547: "IEEE Standard for Interconnecting Distributed Resources with Electric Power Systems," 2008.
[31] C. Parikshith and J. Vinod, "Filter Optimization for Grid Interactive Voltage Source Inverters," *IEEE Trans. Ind. Electron*., vol. 57, no. 12, pp. 4106-4114, 2010.
[32] H. Zheng, Z. F. Liang, M. S. Li, K. Li, "Optimization of Parameters for LCL Filter of Least Square Method Based Three-phase PWM Converter," *Journal of Electrical Engineering and Technology*, vol. 10, no. 4, pp. 1626-1634, Jul. 2015, doi:10.5370/JEET.2015.10.4.1626.
[33] I. Horowitz, "Survey of quantitative feedback theory," *Int. J. Robust Nonlinear Control*, vol. 11, no. 10, pp. 887-921, 2001.
[34] C. Borghesani, Y. Chai and O. Yaniv, "The QFT Frequency Domain Control Design Toolbox for use with Matlab, User's Guide," Terasoft, Inc., 2003.
[35] S. Srikanthan, M. K. Mishra and R. K. V. Rao, "Improved Hysteresis Current Control of Three-level Inverter for DSTATCOM Application," *IET Power Elect*., vol. 2, no. 5, pp. 517-526, 2009.
[36] R. Abu-Hashim, R. Burch, G. Chang, M. Grady, et al., "Test Systems for Harmonics Modeling and Simulation," *IEEE Trans. Power Del*. vol. 14, no. 2, pp. 579-585, Apr. 1999, doi: 10.1109/61.754106.
[37] "Green Technology-Cleantech and Renewable Energy News and Analysis," http://www.greentechmedia.com/articles/read/ionex-has-a-1-mw-battery-ready-for-the-grid, accessed 30 september 2015.

Nomenclature

C	The harmonic filter capacitance
DW	The noise amplitude controlling parameter
F_0	The turbulence scale
F(s)	The prefilter transfer function
G(s)	The controller transfer function
K	The surface drag coefficient
L_1 and L_2	Harmonic filter inductances
N_0	The probability density function counter limit
P_{wind}	The actual wind active power generation
$P_{windref}$	The reference active power
P(s)	Plant model transfer function
R(s)	Reference signal laplace transform
V_{PCC}	Measured rms voltage of the point of common coupling (PCC)
V_{PCCref}	The PCC reference rms voltage
Y(s)	Output of control loop
f_{sw}	Inverter switching frequency
i_{dinj}	The d-component of the injected current
i_g	Grid side inverter current
i_i	Inverter output current
i_{qinj}	The q-component of the injected current
u	The mean wind speed value
u_g	Grid voltage
ui	Inverter output voltage
φ	A random variable with uniform probability density on the interval 0 to 2π
ω_r	Resonance frequency

Appendixes

A. Harmonic filter parameters

Parameters of the designed harmonic filter components are shown in Table 1.

Table 1. Harmonic filter parameters

Parameter	L_1 (mH)	L_2 (mH)	C (μF)	f_1 (Hz)	f_r (Hz)	f_{sw} (kHz)
Value	20	1	25	50	1000	10

B. Wind turbine-generator parameters

Parameters of the variable-speed wind turbine with induction generator in PSCAD software are shown in Table 2.

Table 2. Wind turbine-generator parameters

Parameter	Value
Induction machine rated power	2 MW
Induction machine rated voltage	0.7 kV
Induction machine Stator resistance	0.066 pu
Unsaturated magnetizing reactance	3.86 pu
Mechanical rotational damping	0.008 pu
Stator unsaturated leakage reactance	0.046 pu
Rotor resistance	0.1 pu
Wind turbine rotor radius	40 m
Wind turbine blade area	5026 m^2
Air mass density	1.23 kg/m^3
Rated power of the transformer	2.5 MVA
Rated voltage of primary winding of the transformer	0.7 kV
Rated voltage of secondary winding of the transformer	13.8 kV
Leakage reactance of the transformer	0.04 pu

C. Parameters of the noise component of the wind speed

The Parameters of the noise component of the wind speed in PSCAD software are shown in Table 3.

Table 3. The noise component of the wind speed parameters

Parameter	Value
Number of noise components	50
Noise amplitude controlling parameter	1 rad/s
Surface drag coefficient	0.001
Turbulence scale	30
Random seed number	8
Time interval for random generation	0.5 s

D. Abbreviations and acronyms

BESS	Battery Energy Storage System
DER	Distributed Energy Resources
DES	Distributed Energy Storage
DFIG	Doubly-fed Induction Generator
DG	Distributed Generation
DSTATCOM	Distribution Static Compensator
ESS	Energy Storage Systems
FESS	Flywheel Energy Storage Systems
FSWT	Fixed Speed Wind Turbines
HCC	Hysteresis Current Control
IWD	Intelligent Water Drops
LVRT	Low Voltage Ride Through
PCC	Point of Common Coupling
PID	Proportional-Integral-Derivative
QFT	Quantitative Feedback Theory
SA	Simulated Annealing
SC	Super-Capacitor
SMES	Superconducting Magnetic Energy Storage
VSC	Voltage Source Converter
WG	Wind Generator
WT	Wind Turbine

Mohammad Mahdianpoor He was born in Yazd, Iran on April 21, 1984. He received the B.Sc. degree in electrical power system engineering from Shiraz University, Shiraz, Iran, in 2007. He also received the M.Sc. degree from University of Isfahan, Iran, in electrical power engineering in 2010. He is now the PhD student of power engineering at University of Isfahan. His research interests are distribution and power system control and modeling, power quality and power electronics.

Arash Kiyoumarsi He was born in Shahrekord, Iran, in 1972. He received the B.Sc. degree in electronics engineering from Petroleum University of Technology (PUT), Ahwaz, Iran, in 1995. He received the M.Sc. and Ph.D. degrees in electrical power engineering from Isfahan University of Technology (IUT), Isfahan, Iran, in 1998 and 2004, respectively. In March 2005, he joined the University of Isfahan, Isfahan, as an Assistant Professor of electrical machines, where he became an Associate Professor in 2012. He was a Postdoctoral Research fellow of the Alexander-von-Humboldt Foundation at the Institute of Electrical Machines, Technical University of Berlin, in 2006 and 2007. He received the best teachers' award at the University of Isfahan, in the year 2013. He was also a Visiting Guest Professor at the Institute of Electrical Machines, RWTH, Aachen University, in July 2014. His fields of interest consist of the application of the time-stepping finite element analysis in electromagnetics and electrical machines, and the design and analysis of permanent-magnet synchronous motor-drive.

Mohammad Ataei He received the B.Sc. degree from the Isfahan University of Technology, Iran, in 1994, the M.Sc. degree from the Iran University of Science & Technology, Iran, in 1997, and PhD degree from K. N. University of Technology, Iran, in 2004 (joint project with the University of Bremen, Germany-DAAD scholarship) all in control Engineering. He is associate professor at the Department of Electrical Eng. at University of Isfahan, Iran. His main areas of research interest are control theory and applications, nonlinear control, and chaotic systems' analysis and control.

Rahmat-Allah Hooshmand He received the B.Sc. degree from University of Mashhad in 1989, the M.Sc. degree from University of Tehran, Iran and PhD degree from Tarbiat Modarres University, Iran in 1990 and 1995, respectively all in Electrical Engineering. He is currently Professor in Electrical Engineering Department, University of Isfahan, Isfahan, Iran. His main area of research interests are power market, smart grid and modeling of power system and distribution networks.